

FEM ANALYSIS AND EXPERIMENTAL TESTS ON A DEVICE FOR POURING CONCRETE

Gianni Caligiana, gianni.caligiana@unibo.it

Alfredo Liverani, alfredo.liverani@unibo.it

Luca Boschi, welld@libero.it

DIEM, Faculty of Engineering, Viale Risorgimento, 2 – 40136 Bologna - Italy

Abstract. Aim of the paper is the prediction of the on-service behaviour of an articulated device for pouring concrete composed of five arms. Experimental tests have been performed on a prototype of the equipment made on Weldox 900E steel, while a parallel finite element analysis has been made on a virtual model of the device. Comparison of experimental tests and numerical analysis allows to gain a deep insight on the performance of the apparatus. A virtual model of the apparatus has been developed by a 3D CAD modeller and analyzed through FEM numerical programs in both static and dynamic conditions. During dynamic simulation, accurate evaluation of all loadings and constraints have been made and a modal analysis has been performed on the whole structure to identify critical frequencies. Test plans have been devised to assess performance of the articulated device in both static and dynamic conditions by instrumenting the prototype of the equipment with rectangular rosettes. During quasi-static tests, a series of known discrete loads (up to roughly 1800 N), measured by a dynamometer, has been applied at the end of the fifth arm of the structure. Deflections at the end of the fifth arm, corresponding to each applied load, have been measured by a laser device, utilizing, as reference, the configuration at rest of the structure. Strains are measured by the strain gages of each rosette. Dynamical tests have been performed, by simulating experimentally concrete pouring. During both static and dynamic tests, the 3D strain state and the 2D plane stress state can be derived in each site where rectangular rosettes have been located. Principal stresses, principal strains, direction of the principle strains and stresses, Mohr stress and strain circles have been recorded and compared with those predicted through the finite element analysis. Comparison between numerical and experimental results has been carried out. A very good correlation has been obtained for static loading to assess the soundness of the virtual model. Both experimental tests and numerical simulation in the on-service condition allow to identify the more dangerous resonance frequencies for the structure and offer some interesting suggestions for design improvement of the whole device or of its components.

Keywords: design, 3D modelling, virtual models, shape optimization, finite element analysis, dynamic loading.

1. INTRODUCTION

Concrete pouring in the construction of buildings, dams, bridges, roadways, etc., is a conventional activity. It is performed to obtain foundations, walls, beams, building slabs, reinforced surfaces on solid, well-drained bases to support heavy loads like vehicles. This operation must be often carried out in a not-comfortable way, while trying to reach all significant sites. Present technology supports the operator by means of transportable devices to perform this task. They are articulated frames, composed of several arms, holding a piping system with an ending hose to pour concrete (Fig. 1a and Fig. 1b).

Beginning from the current state of art of equipments for pouring concrete, an extensive study in this area has been undertaken at DIEM Department (Malpensa, 2009). Attention has been paid to a five-arm articulated device prototype produced in Romagna countryside (Fig. 1a). The equipment is made by beams of Weldox 900 E steel (S890QL) (SSAB, 2009; Martinez *et al.*, 1997), with hollow rectangular cross sections. In its fully extended configuration, it is 58-meter long. Each arm is pin-joined to the preceding one (Fig. 1a). On service, hydraulic cylinders allow relative motion of each of the five arms with respect to the adjoining one. Each arm is suitably shaped and, at rest, it can be folded upon the preceding one, resulting in a whole assembly, which can be carried by a suitable tractor unit (Fig. 1c).

A deep CAD modelling activity (Mortenson, 1997; Rooney, 1997) has been implemented through 3D modellers. Particular care has been devoted to remove model clearances and imperfections (Brüderlin, 1998; Farin, 2002), leading to reliable virtual models for successive finite element analysis (Zienkiewicz, 2005; Cook, 1995; Moaveni, 2003; Stolarski, 2006). Detailed constructive 2D drawings have been derived from the 3D model, but this part of the work is not included here, because it is beyond the scope of the paper.

Test plans have been implemented on the prototype of the equipment. The prototype has been instrumented with twelve rectangular rosettes (Dally, 2005). They have been glued in significant sites, identified through the finite element analysis. Rosettes are located in areas characterized by quite elevated stresses and strains but, contemporarily, by gradients not so high, to provide unreliable strain readings.

Static tests have been devised to prove the soundness of the predictions made by FEM analysis through the virtual model. Discrete loadings have been applied at the end of the fifth arm, corresponding strains have been recorded by strain gage rosettes and deflections have been measured by a laser device.

Dynamical tests have been performed, by simulating pouring of concrete. Two pumping frequencies are considered (22 strokes/min and 26 strokes/min). Accurate study of stresses and strains recorded during experimental tests testifies, as expected, that dynamical actions are much more critical for the structure than static ones.



Figure 1a. Prototype of the five arm device produced in Romagna (the piping system to pour concrete can be easily seen).



Figure 1b. Example of a commercial device to pour concrete in an on-service configuration.



Figure 1c. Example of the folded assembly of an equipment for pouring concrete, carried by a suitable tractor unit.

Paper is articulated in paragraphs (marked in the followings by §).

- In § 2 a description of the articulated device, of its dimensional characteristics and of the material utilized is given.
- Methodology applied during the implementation of experimental tests is described in § 3.
- Virtual modelling (3D-CAD modelling and finite-element-analysis modelling) is illustrated in § 4.
- Numerical predictions and their comparison with experimental results are reported in § 5.
- Conclusions and future developments are outlined in § 6.

2. MAIN CHARACTERISTICS OF THE PROTOTYPE OF THE ARTICULATED DEVICE

All the five arms of the equipment are made by plates of Weldom 900E steel, assembled to obtain beams of hollow rectangular cross section. The most important properties of this steel are collected in Table 1, 2 and 3. External and internal height and width of the cross sections are often different for different locations, because arms are suitably shaped to allow the assemblage of the folded configuration for transportation and because they are dimensioned by roughly following the theory of a beam of uniform strength in bending. Obviously, economical reasons don't suggest a continuous change in dimensions, but rather a proper discrete change in thickness in several regions, made, for example,

Table 1. WELDOX 900E (S890QL) Steel - Chemical composition.

C*	Si*	Mn*	P	S	B*	Nb*	Cr*	V*	Cu	Ti*	Al* total	Mo*	Ni	N
max %	min %	max %	max %	max %										
0,20	0,50	1,60	0,020	0,010	0,005	0,04	0,70	0,06	0,10	0,04	0,018	0,70	0,10	0,015

* Intentional alloying elements. The steel is grain-refined.

Table 2. WELDOX 900E (S890QL) Steel - Mechanical properties

Tests are performed on transverse test pieces			
Plate thickness (mm)	Yield Strength $R_{p0,2}$ (min.) (MPa)	Tensile Strength R_m (MPa)	Elongation A_5 (min.) (%)
4,0 - 50,0	900	940-1100	12
50,1 - 80,0	830	880-1100	12

Table 3. WELDOX 900E (S890QL) Steel – Impact Properties.

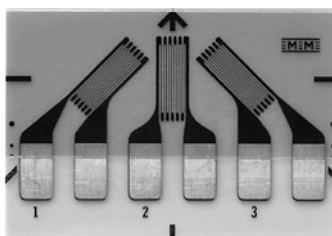
Tests are performed on transverse ⁽¹⁾ Charpy V 10 x 10 test specimens ⁽²⁾			
Test temperatures (°C)	0	- 20	- 40
Impact energy (J)	35	30	27

⁽¹⁾ Transverse impact testing according to EN 10025, option 30, will apply.

⁽²⁾ For plate thickness less than 12 mm, subsize Charpy V-specimens are used. The specified minimum value is then proportional to the cross section of the specimen.



Figure 2. Example of a cross section at the root of arm I near the tractor unit.



a)



b)



c)



d)

Figure 3. a) Example of the rectangular rosette utilized.
b), c) and d) Some steps of the set-up of strain rectangular rosettes.

by applying reinforcement slabs welded in suitable locations, chosen by the designer.

In the paper, the arms of the equipment have been numbered with roman numbers, starting from the first arm (arm I, the nearer to the tractor unit). Figure 4 shows a scheme of the whole structure in its extended configuration (58 meters).

Figure 2 shows the dimensions of the largest cross section, chosen just nearby the tractor unit (at the root of the whole structure).

3. EXPERIMENTAL TEST IMPLEMENTATION

3.1. Rectangular rosette location

Twelve rectangular rosettes have been glued in suitable sites (Fig. 4), chosen on the basis of finite element method (FEM) preliminary results. Rosettes have three strain gages at 0° , 45° and 90° (Fig. 3a). Attention has been paid to align the central strain grid (gage 2 at 45°) along the beam symmetry axes of each arm. Figures from 3b to 3d illustrate some steps of the set-up of strain rectangular rosettes. Main loading in the whole structure is due to bending, therefore rosettes have been generally located in the upper and lower surfaces of the beam of each arm (the areas farther from the neutral axes). Finite element analysis has shown that large areas of arm I are subjected to uniform bending and they are far from significant stress raisers. These regions can be particularly useful to obtain reliable experimental results that can be used as reference to calibrate the virtual model and to check FEM results. As a consequence, A and C rosettes have been located in suitable sites in the upper surface of arm I, while B rosette has been placed on the lower surface of arm I (Fig. 4). The third arm (arm III) is in the middle of the equipment, so it has been shaped according to a curved geometry much more than the others, to allow the folding operation before any transportation of the whole articulated device (§ 1 and Fig. 1c). Owing to its peculiar contour, strain recording in some areas of the third arm is strongly recommended. D and E rosettes have been located in the upper surface of arm III and F rosette on its lower face.

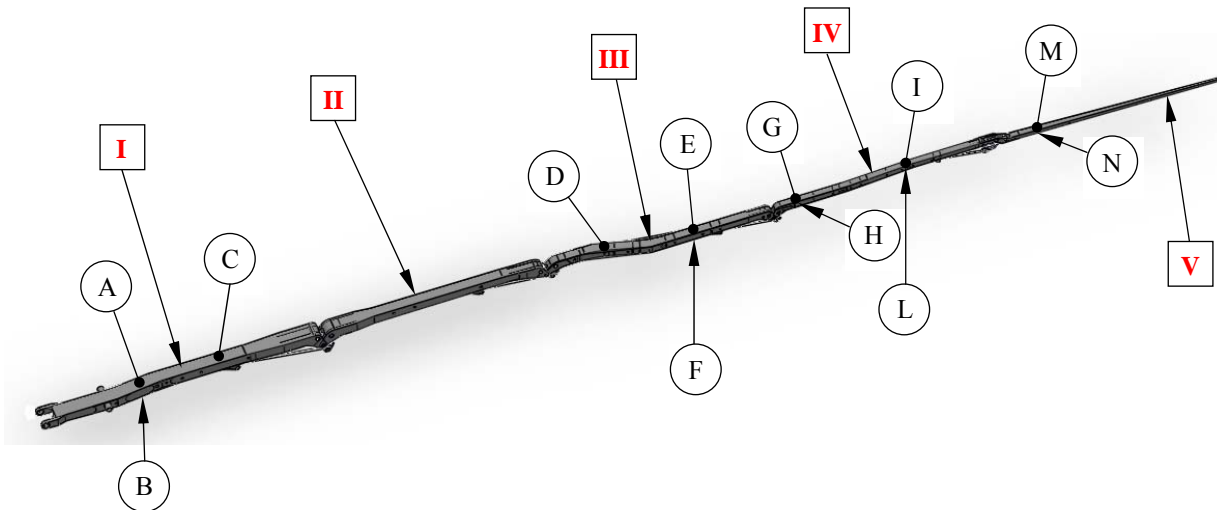


Figure 4. Location of the twelve rectangular rosettes in the five arms of the device.

Arms IV and V have progressively smaller sections (according to the approach of beam of uniform strength in bending mentioned in § 2) and they have some stress and strain raisers. Rosettes have been located in those sites, where critical situations have been held in evidence by finite element analysis (§ 5). G and I rosettes have been put on the upper surface of arm IV, H and L, respectively, on the lateral and lower surface of arm IV. M rosette has been located on the upper surface of arm V and N rosette on its lateral surface. Whenever critical areas have been chosen, suitable distance from extreme strain raisers has been maintained, to let sufficient reliability for all rosette strain readings.

3.2. Experimental tests: methodology and tools

Experimental results are recorded by an eight channel Esam Traveller plus device (ESAM, 2000). Each strain gage of each rectangular rosette is connected through an half Wheatstone bridge to the corresponding strain gage of the rosette used for temperature compensation. Full Wheatstone bridge has been obtained by suitably connecting the half bridge to the Esam Traveller device circuits. Thus, bridge balancing and successive recording of the experimental information can be performed. Results have been elaborated through the resident device (ESAM, 2000), but, owing to some deficiencies in the native program, “ad hoc” numerical modules have been written by one of the authors in Mathematica® language, Version 6 (Wolfram, 1999). Some of the final output of the numerical program are 3D Mohr circles, which very efficiently visualize static and dynamic situations of each measurement section (Durelli).

3.3. Quasi-static preliminary calibration tests

Preliminary quasi-static tests have been performed on the prototype of the articulated device, in its extended configuration (Fig. 4). Discrete known loads, measured by a dynamometer (60 kg \approx 588 N, 90 kg \approx 883 N, 120 kg \approx 1177 N, 150 kg \approx 1471 N, 180 kg \approx 1765 N), have been applied at the end of the fifth arm of the structure. Deflections at the end of the last (fifth) arm corresponding to each applied load have been measured by a laser device, using, as reference, the configuration at rest of the structure (positive values correspond to downward deflections, Fig. 5).

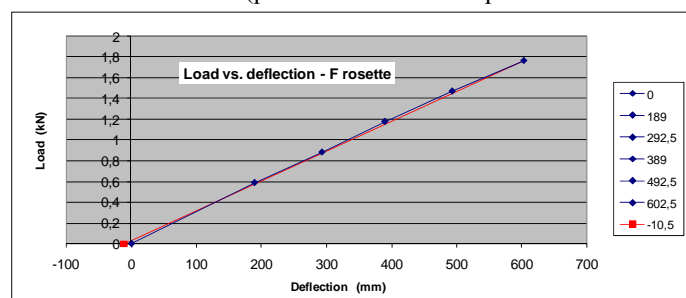


Figure 5. Quasi static tests: experimental load-versus-deflection curve measured at the end of the fifth arm (arm V of Fig. 4).

In each site where rectangular rosettes are present, the 3D strain state and the 2D plane stress state can be derived (Fig. 6). Principal stresses, principal strains, directions of the principle strains and stresses, Mohr stress and strain circles have been recorded and compared with those predicted through the finite element analysis (§ 5). In Fig. 6a, the

axis in red corresponds to the x-axis, the direction of the strain gage 1 (Fig. 3a) of rosette “L”, while blue axis is the direction of the y-axis, the direction of the strain gage 3 (Fig. 3a) of rosette “L”. Obviously, the two orthogonal axes results, as expected, at 180° inside the Mohr circle.

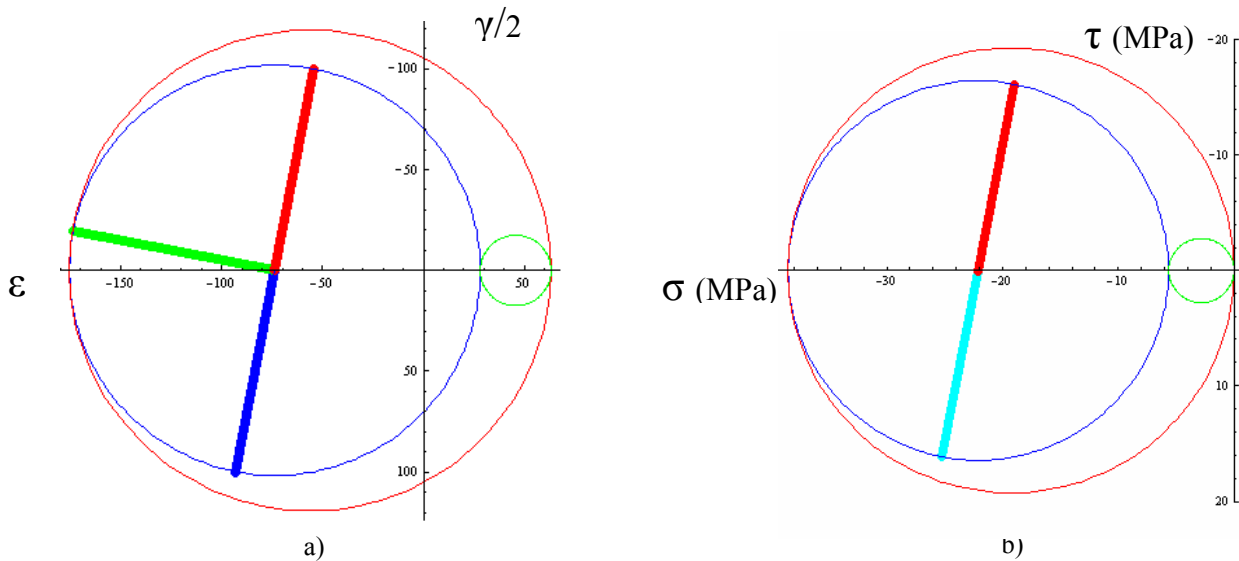


Figure 6. Quasi-static tests: a) Mohr strain circle (on the left) and b) Mohr stress circle (on the right) obtained by results from “L” rectangular strain gage rosette during quasi-static tests.

3.4. On-service dynamical experimental tests

A second plan of dynamical tests has been performed, by simulating pouring of concrete. Two (medium and high) pumping frequencies are considered: 22 strokes/min (0,37 Hz, corresponding roughly to 125 m³/h) and 26 strokes/min (0,43 Hz, corresponding roughly to 150 m³/h). Pseudo random strain histories can be recorded by rectangular rosettes (Fig. 7). Actually, histories show almost periodic peaks of similar amplitude (even if not exactly identical one to each other) at correspondingly analogous intervals of time. Experimental results lead to the knowledge of stresses, strains, principal directions and Mohr circles as a function of time. Inside the pseudo random history, accurate study of stress and strain circles of maximum diameter (normally corresponding or very near to a maximum of the strain history), testifies, as expected, that dynamical actions are much more critical for the structure than static ones (Fig. 8). Comparison of Fig. 6 and Fig. 8 shows that the principal directions don’t vary significantly, while switching from static to dynamic loading.

The frequency response (resonance) of the structure to the action of the pumping frequencies seems very important for structure strength as testified by experimental tests and confirmed by finite element analysis (see § 5.3).

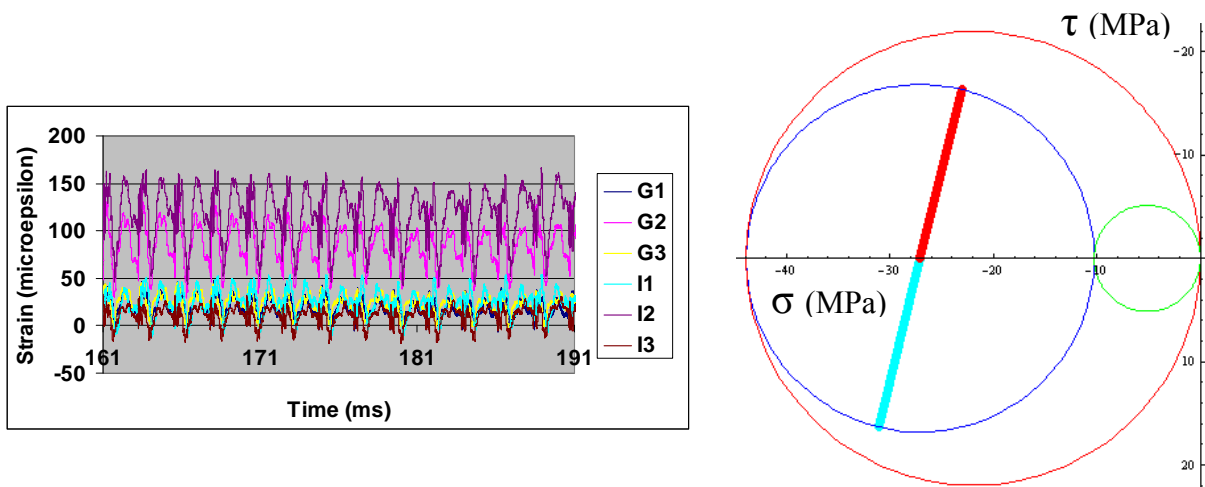


Figure 7. Strain histories recorded by each strain gage of “G” and “I” rosettes during simulated on-service (dynamic) condition, at the maximum pumping frequency.

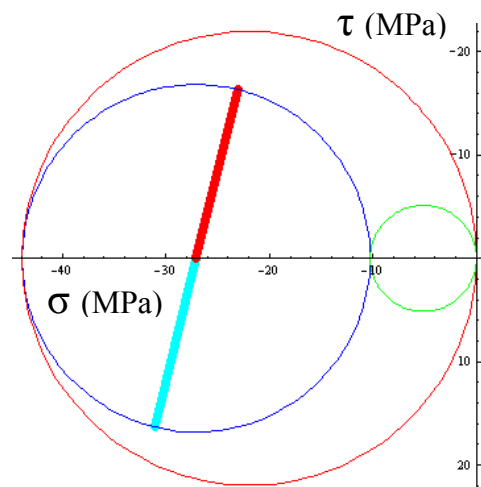


Figure 8. Maximum diameter stress circle obtained at medium pumping frequency during the dynamical history for rosette “L”.

4. VIRTUAL MODELLING SET-UP

A numerical 3D model of the prototype of the 58-meter articulated device (§ 1 and § 2) has been implemented by CAD software. As it has been already stated (Fig. 4), the arms of the virtual model of the articulated device have been numbered progressively starting with the arm which is nearer to the tractor unit. Actually, activity consists in an accurate re-modelling of existing virtual prototypes of each arm of the device to remove clearances, interferences or shape imperfections in general, with the aim to avoid bugs or malfunctions during successive finite element analysis. Mutual actions between arms caused by hydraulic rams and appropriate constraints on the contact surfaces have been properly simulated (§ 4.2, Malpensa, 2009). Virtual models have been imported inside FEM software environment (MD Patran, R2.1, and MD Nastran, R3) to perform finite element analysis (Moaveni, 2003; Stolarski, 2006).

4.1. Meshing

During the first rough automatic meshing performed by commercial FEM codes, ten-node tetrahedral isoparametric elements have been utilized. Owing to the complex geometry of the structure, local mesh refinements have been performed in peculiar regions. A proper set-up to ascertain mesh fine-tuning and element shape quality has been imposed. Convergence tests have been performed to assess the achievement of a reliable solution (see § 5.2).

Furthermore, the geometric model has been re-arranged to implement a mesh with four-node, bilinear thick-shell elements, more suitable to solve the particular problem (§ 5.1). As an example relative to the fifth arm, a solution achieved in static conditions, with a mesh of 74890 shell elements (with main element length of 10 mm), needs a computation time (comprehensive of mesh input data, stiffness matrix assembling, constraint settling, equation system solution and output file creation) of 1165 seconds. A solution with a mesh of 19655 shell elements, with main element length of 20 mm, needs a computation time of 35 seconds, while a solution with a mesh of 6162 shell elements, with main element length of 40 mm, needs a computation time of 10 seconds.

4.2. Virtual modelling of loading and constraints

The arms of the device have often complex shapes (Fig. 10), owing to the fact that each section must be able to be articulated and piled up on the preceding one to achieve a unique stack of five arms, which can be easily supported and carried by a tractor unit or a specialized lorry. Structural loadings due to arm's own weight have been applied in the centre of mass of each section. This item is comprehensive of accessories and welds, which constitute about 7% of the total mass. The resultant forces of structural loadings due to the piping system to pour concrete, with the weight of concrete added up, have been applied in the suitable points of the structure, where ducts are actually joined. The mass of all link devices to allow arm movements have been considered. In static tests, each arm has been considered by itself and the actions applied by other arms are properly calculated (Fig. 9; Malpensa, 2009). This task has been performed by starting from the last arm (arm V) and then coming backwards to the first one (arm I). Figure 9 shows the scheme of loads and reactions applied to the fifth arm. Figure 10 illustrates loadings and constraints for the virtual model of the third arm, ready for FEM analysis.

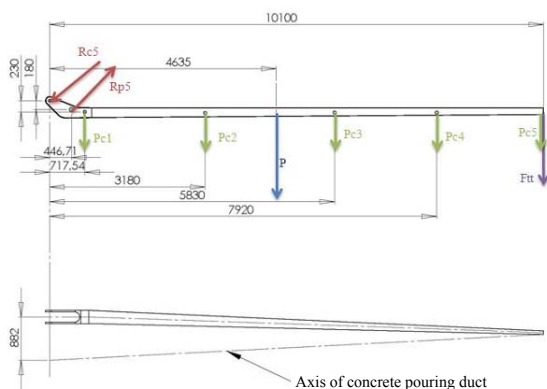


Figure 9. Scheme of loadings and reactions applied to arm V.

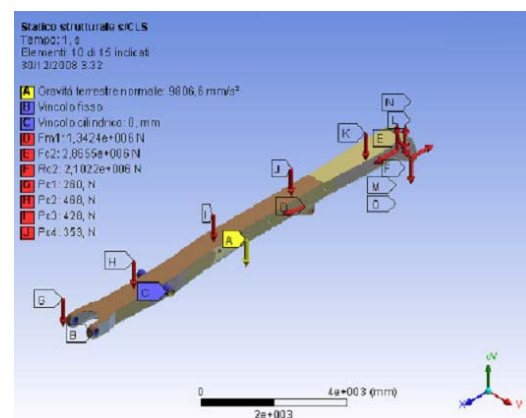


Figure 10. FEM virtual model of arm III (with loads and constraints properly evidenced).

4.3. Set-up for the comparison of FEM and experimental results

Virtual probes have been located on the FEM model to derive stress and strain values in the same locations (Fig. 11b and 11c), where rectangular strain rosettes on the prototype have recorded experimental results (Fig. 11a).

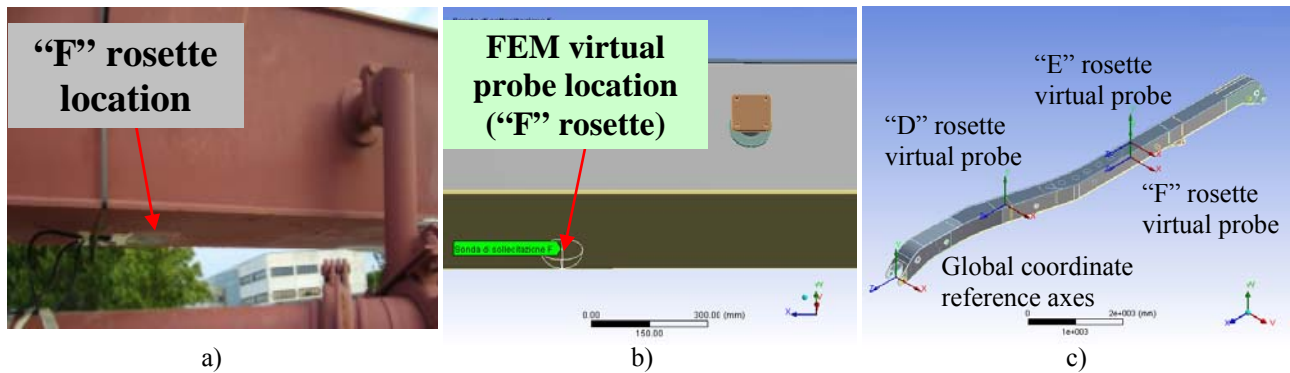


Figure 11. Examples of rectangular rosette location: a) location of “F” rosette on the real prototype of the apparatus; b) location of “F” rosette virtual probe on the virtual model; c) location of the virtual probes on the third arm.

5. NUMERICAL PREDICTIONS: RESULTS AND COMPARISON WITH EXPERIMENTAL RESULTS

5.1. Quasi-static tests: methodological approach in the comparison of experimental and virtual-probe results

FEM results have evidenced in all cases that stresses recorded numerically are almost everywhere well below the yield strength of the material and strains are entirely within the elastic field. Owing to the linearity of the problem, the maximum weight hanged up, during static experimental tests, at the end of the fifth arm (§ 3.3), have been considered directly in the analysis of the quasi-static condition. Moreover, the maximum value of 1765 N (\approx 180 kg) corresponds roughly to the weight of the ending part of the duct for pouring concrete, completely filled with concrete.

On the experimental counterpart, strain rosettes have been glued on the apparatus already assembled. So, Wheatstone bridge circuit of the rosette strain gages has been balanced to zero, while structural loadings were obviously already on. Low strain condition could allow the application of the superposition principle. Nevertheless, to avoid the suspect of geometrical nonlinearities, an analysis of the displacements must be considered. Resulting deflections are significant, but completely negligible if compared with the length of the arms or of the whole structure (58 meters). Once and for all, two FEM program runs have been performed for the fifth arm, to ascertain the lack of geometric nonlinearities: the former with both structural and external loadings (of 1765 N), the latter with only structural loadings. The difference between them represents the situation of the application of external loadings to an already deformed structure (identical to the experimental one). This result has been compared to a FEM run performed by simply applying the only external loading to the original frame. Comparison is not shown here, but it leads to almost coincident results, testifying the uselessness of the previous much more involved analysis. So, in the FEM analyses of all the consecutive arms, static test external loading has been applied to the end of the fifth arm, simply ignoring the frame structural loads.

Comparison has been made on terms of principal stress and strain values, direction of principal stresses and strains, equivalent stress and strain values. An impressive compendium of the comparison between numerical predictions and experimental results through Mohr circles can be seen, for the “C” rosette, in Fig. 12 and 13.

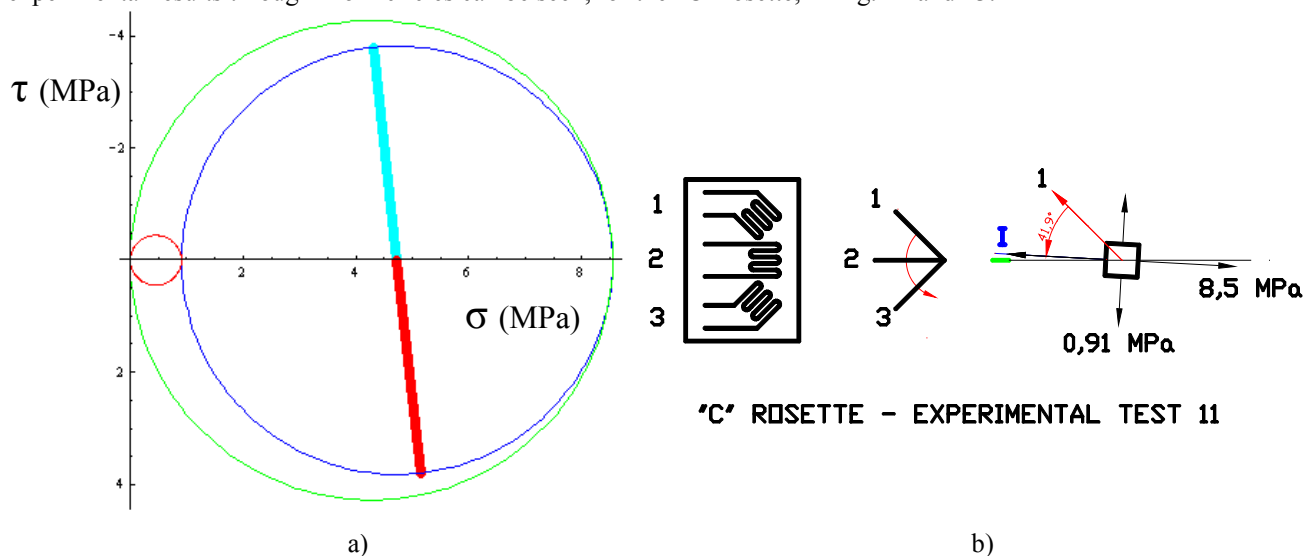


Figure 12. a) Stress Mohr circle and b) principal stress directions obtained experimentally by “C” rosette (axis in red corresponds to the direction of the first strain gage of the rectangular rosette, Fig. 3a).

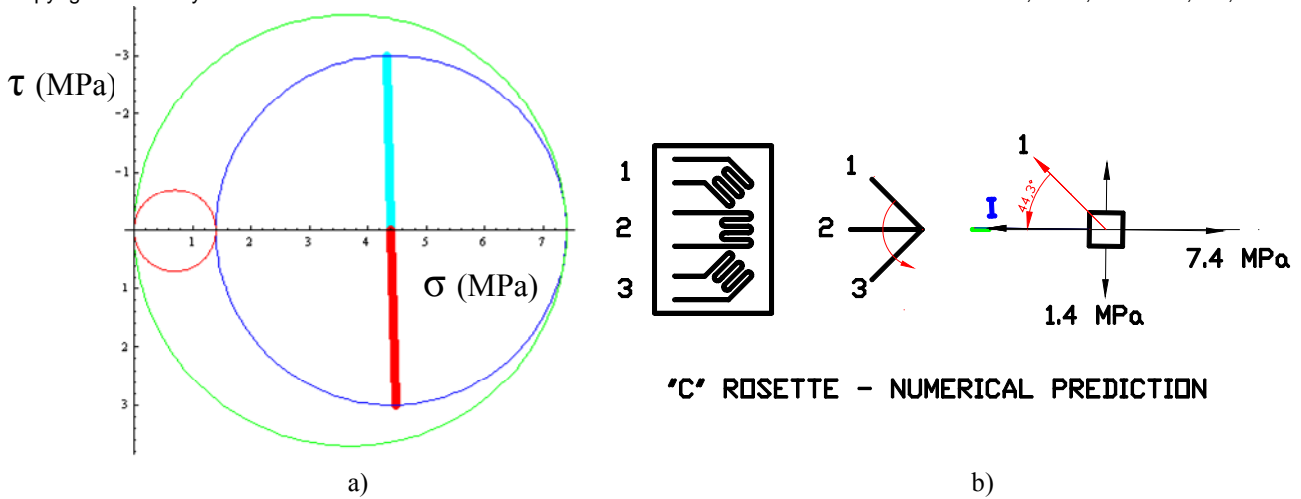


Figure 13. a) Stress Mohr circle and b) principal stress directions predicted numerically by a virtual probe located on the virtual model in the same position of "C" rosette (axis in red corresponds to the direction of the first strain gage of the rectangular rosette, Fig. 3a).

In Fig. 14, FEM results for the fifth arm are shown. They are obtained with a shell-element meshing (§ 4.1), in quasi-static conditions, with an applied loading at the end of the fifth arm of 1765 N. In Fig. 15, a comparison is shown of Von Mises equivalent stresses, derived by the finite element analysis, with those obtained experimentally, for some rosettes of the fourth and the fifth arms, in the before mentioned quasi-static condition.

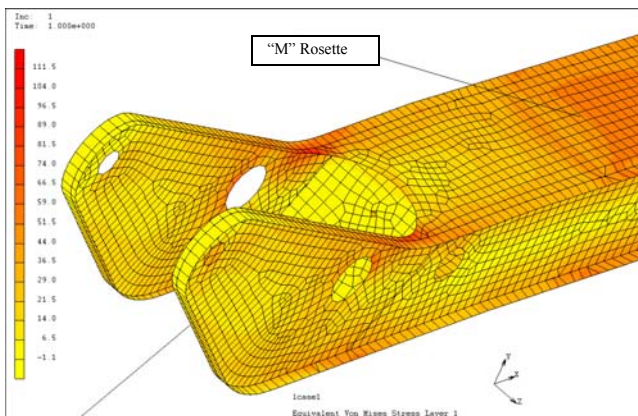


Figure 14. Arm V. Finite element analysis results. Map of Von Mises equivalent stresses (location of the virtual probe for "M" rosette is evidenced).

Von Mises equivalent stress (MPa)				
Arm	Rosette	Experim.	F.E.M.	Error (%)
IV	G	29	31,1	7,2
IV	H	17,6	18,6	5,7
IV	I	41	43,1	5,1
IV	L	36	42,8	18,9
V	M	45,3	42,9	5,3

Figure 15. FEM numerical analysis predictions and experimental results for Von Mises stresses in quasi-static condition (1765 N applied load at the end of the fifth arm).

5.2. Quasi-static tests: convergence analysis

Convergence analysis has been performed to verify the soundness of finite element mesh, by using numerical predictions for quasi-static tests. Three different mesh refinements have been considered (Fig. 16a, 16b and 16c). The first mesh (Fig. 16a) is obtained automatically (but with the proper parameter set-up described in § 4.1), while a reduction of almost 1/3 in element size results when going from the mesh of Fig. 16b to that of Fig. 16c.

A clear trend can be seen in Fig. 16d for "F" virtual probe located in the third arm of the virtual model of the articulated device. Numerical predictions show how a sufficiently accurate mesh refinement allows stress and strain results to converge towards experimental results, testifying the accuracy of FEM virtual modelling.

As a comparison, Figure 14 shows an example of the mesh obtained with bilinear thick shell elements with four nodes and six degrees of freedom per node (three displacements and three rotations) for the fifth arm.

5.3. Dynamical tests: modal analysis

Strain rosettes have been glued on the equipment already deformed by its structural loadings and, in this condition, Wheatstone bridge circuit has been balanced. To ensure comparable configurations for experimental and numerical

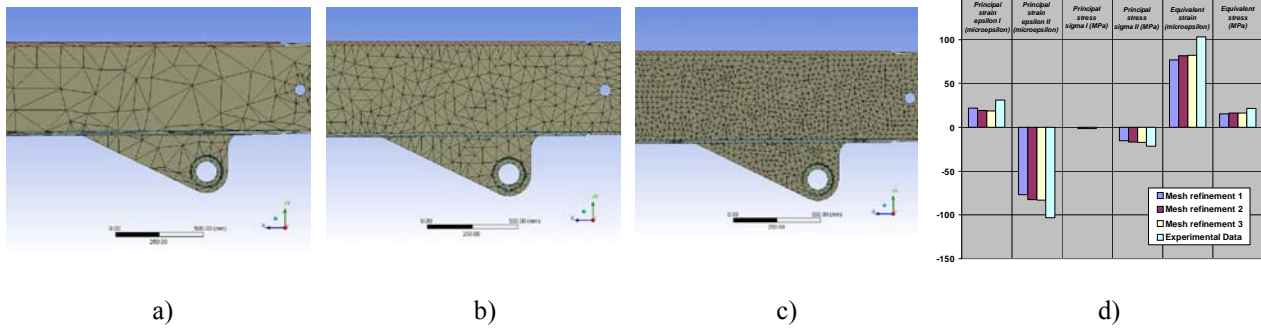


Figure 16. FEM convergence test: Influence of mesh refinement on numerical predictions.

analyses, two finite element program runs have been performed, the former, with only structural loadings (and without external loadings), the latter, with both structural and external loadings applied during dynamical experimental tests.

Accounting to the superposition principle, the outcome resulting from the difference between the second and the first FEM runs is considered as the numerical prediction to be directly compared with the experimental results. This approach is particularly useful in the modal analysis performed during the modelling of the dynamical concrete-pouring loading.

Starting from the knowledge of the mass flow rate of concrete and from the number of strokes per minute at two different working regimes (medium and high, § 3.4), motion equations have been settled to obtain axial forces transferred by friction to the duct of concrete and, consequently, to the device (the duct is joined to each arm in several points, Fig. 1a).

Dynamic loadings have been properly added to the structural ones and a single virtual model of the whole structure has been implemented, instead of several model for each arm, as in the quasi-static analysis. Actually, the presence of alternating forces implies oscillating reactions too, to be exchanged between arms; so, all the components must be examined, in a whole, at the same instant of time, leading to the need of a unique model for the complete structure. Each junction between arms has been accurately examined (also manually if necessary) and properly modelled.

A modal analysis (Clough, 1993) of the whole structure has been carried out (Fig. 17a) to obtain the mode shapes and frequencies of the articulated device. A critical value of frequency of 1,1 Hz was identified. It corresponds to the critical frequency of the second mode of vibration in bending on an horizontal plane. The mode shape configuration of the whole structure shows critical areas in the curved shaped region of the third arm and at the root of the fifth arm (arms are numbered starting with the arm nearer to the tractor unit, according to the scheme of Fig. 4).

Frequency analyses performed during experimental tests are shown in Fig. 17b, for the three strain gages of “A” rosette and the three strain gages of “C” rosette of the first arm at the highest pumping frequency (0,43 Hz), and in Fig. 17c, for the three strain gages of rosettes “D” and “E” of the third arm at medium pumping frequency (0,37 Hz).

All the time, in the experimental results, a frequency peak as a response to the almost periodic pumping loading can be always seen at about 0,37 Hz, for medium pumping frequency, and at about 0,43 Hz, for the highest pumping frequency. In both cases, a further very high peak can be found (both numerically and experimentally) at about 1 Hz. This peak corresponds to 1,1 Hz for the third (Fig. 17c) and fifth arm (not shown). Consequently, comparison of numerical results with experimental ones shows a striking correlation.

In fact, as shown by the numerical analysis (Fig. 17a), 1,1 Hz seems to be the most dangerous frequency for the entire structure. It corresponds to a vibration mode on an horizontal plane, excited by the pumping loading. On the contrary, during the static analysis, maximum stresses appear to originate mainly from bending on a vertical plane, which is a loading action more intuitive to understand (just giving a first glance to the structure of the articulated device).

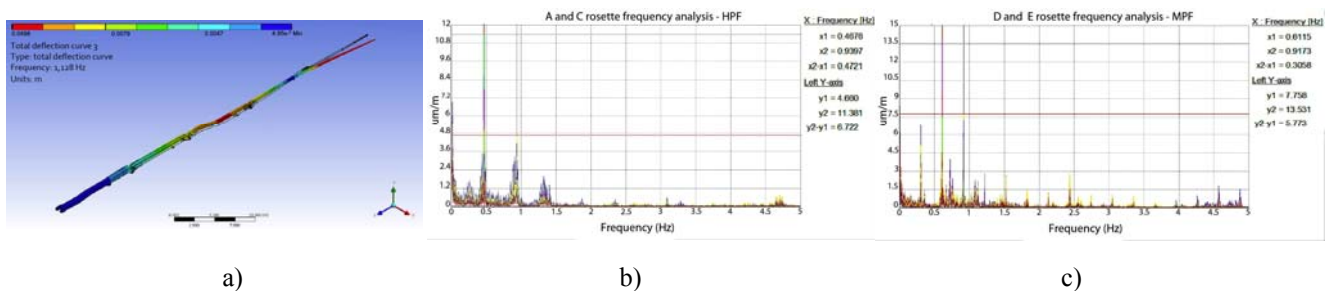


Figure 17. a) FEM modal analysis; b) - c) frequency analysis of experimental results: rosettes “A” and “C” of arm I at the highest pumping frequency (plot b) and rosettes “D” and “E” of arm III at medium p. f. (plot c).

6. CONCLUSIONS AND FUTURE DEVELOPMENTS

A sound model to analyze an articulated device for pouring concrete has been developed and validated experimentally. Stresses and strains in both quasi-static and on-service conditions have been evaluated numerically and compared with the experimental results. The comparison of numerical and experimental results in on-service condition, at medium and high pumping speed, shows a very good correlation, allowing to identify the more dangerous resonance frequencies for the structure (around 1 Hz). This frequency, which is the response to the forcing frequency of the pumping action, suggests that resonance is the more critical aspect to be checked in service for the apparatus. Actually, structural loadings cause negligible stresses if compared with the allowable strength of the Weldox 900 E steel used.

This work offers several suggestions for future activities in this field, like: a) the study of the proper geometrical modification of the existing prototype and of its components (shape optimization), b) the use of fatigue commercial programs or the implementation of “ad hoc” numerical programs for endurance predictions of the different mock-ups of this kind of articulated devices, c) the set-up of an out-of-service experimental testing rig for assessing the articulated device or its new models or upgrades, by simulating the actual working condition during concrete pumping activity. Doctoral dissertation, first and second level degree theses are going on about these theme under the authors’ guide.

7. ACKNOWLEDGEMENTS

Authors are very grateful to Ing. Franco Menapace and to Ing. Paolo Proli for their support in this research activity.

8. REFERENCES

- Brüderlin, B., Roller, D., 1998, “Geometric Constraint Solving and Applications”, Springer-Verlag, Berlin Heidelberg, Printed in Germany, 3-540-64416-4, 301 p.
- Clough, R.W., Penzien, J., 1993, “Dynamics of Structures”, Mc Graw Hill Book Co., International Edition, ISBN 0-07-113241-4, 738 p.
- Cook, R. D., 1995, “Finite Element Modeling for Stress Analysis”, John Wiley & Sons, Inc., 315 p.
- Dally, J. W., Riley, W. F., 2005, “Experimental Stress Analysis”, Fourth edition, College House Enterprises, LLC 5713 Glen Cove Dr. Knoxville, TN 37919-8611, ISBN 0-9762413-0-7, 571 p.
- Durelli, A. J. , Phillips, E. A., Tsao, C. H., “Introduction to the Theoretical and Experimental Analysis of Stress and Strain”, McGraw-Hill Book Co., Inc., Ney York, 497 p.
- ESAM Traveller plus, 2000, Measurement System, Technical Manual, 63 p.
- Farin, G., 2002, “Curves and Surfaces for CAGD, a practical guide”, Academic Press, Hartcourt Place, 32, Jamestown Road, London, NW1 78Y, U.K., ISBN 1-55860-737-4, 491 p.
- Malpensa, G., 2009, “Dispositivo articolato per la deposizione del calcestruzzo: modellazione 3D, analisi MEF e confronto con i risultati sperimentali”, first level Mechanical Degree tesi (in Italian), 16 Gennaio 2009, Academic Tutor: G. Caligiana.
- Martinez, L. L., Blom, A. F., Trogen, H., Dahle, T., 1997, “Fatigue behaviour of steels with strength levels between 350 and 900 MPa influence of post weld treatment under spectrum loading”, Proceeding of the North European Engineering and Science Conference, (NESCO), Welded High-Strength Steel Structures, Stockholm, Edited by A.F. Bloom, EMAS Publishing, London.
- Moaveni, S., “Finite Element Analysis Theory and Application with Ansys”, 2003, Pearson, Prentice Hall, Inc., Upper Saddle River, Ney Jersey, ISBN 0-13-191857-5, 822 p.
- Mortenson, M. E., 1997, “Geometric Modelling”, John Wiley & Sons, Inc., United States of America, ISBN 0-471-12957-7, 509 p.
- Rooney, J., Steadman, P., 1997, “Principles of Computer-Aided Design”, UCL Press/Open University, 1-85728-222-1PB.
- Stolarski, T., Nakasone, Y., Yoshimoto, S., 2006, “Engineering Analysis with Ansys Software”, Elsevier Butterworth-Heinemann, Linacre House, Jordan Hill, Oxford, OX2 8DP, 30 Corporate Drive, Burlington, MA 01803, ISBN 0-7506-6875-X, 456 p.
- SSAB web site: <http://www.ssab.com/>
- Wolfram, S., 1999, “The Mathematica Book”, Cambridge University Press, The Pitt Building, Trumpington Street, Cambridge CB2 1RP, UK.
- Zienkiewicz, O. C., Taylor, R. L., Zhu, J. Z., 2005, “The Finite Element Method”, Elsevier Butterworth-Heinemann, Linacre House, Jordan Hill, Oxford, OX2 8DP, 30 Corporate Drive, Burlington, MA 01803, ISBN 0-7506-6320-0, 719 p.

9. RESPONSIBILITY NOTICE

The authors are the only responsible for the printed material included in this paper.